Ripple-Free Boost-Mode Power Supply Using Photonic Power Conversion

Matthew M. Wilkins, Masanori Ishigaki, Philippe-Olivier Provost, Denis Masson, Simon Fafard, Christopher E. Valdivia, Ercan M. Dede, and Karin Hinzer

***Abstract*—Photonic power converters (PPCs) are a class of photovoltaic devices designed for efficient conversion of monochromatic (laser or LED) light to electricity. These devices are composed of multiple p-n junction diodes arranged in a tandem configuration and connected in series. They have reached high energy conversion efficiencies (70%) and areal power densities of 100 W/cm^2. When these devices are illuminated with a high-efficiency diode laser, they can provide isolated dc–dc conversion from the laser voltage ($<$2.3 V) to the open-circuit voltage of the PPC (1.2 to 23 V) with low capacitance and low conducted electromagnetic interference (EMI) compared to conventional switching power converters. The voltage conversion ratio is controlled by varying the number of p-n junctions in the PPC from 1 to 20 in demonstrated designs. In this paper, we demonstrate the use of photonic power conversion within two new applications. First, the laser/PPC unit is applied as a linear photonic boost converter, producing a regulated 12 V output stepped-up from a 3.3 V input to the control board. Output ripple is negligible as compared with a switching boost converter of similar size. Efficiency of this linear, regulated dc–dc conversion system was 12.7%, compared with a 77.6% reference switch-mode converter. Power density was 0.18 W/cm^3, compared with 1.5 W/cm^3 for the reference. Relative to switch-mode power conversion, the photonic technology has lower efficiency and lower power density, but superior isolation and rejection of ripple and EMI. Both technologies are highly scalable. For the second application, the same unit is applied to power a 650-V SiC MOSFET gate driver requiring high galvanic isolation, demonstrating a 20 dB reduction in conducted-current EMI from the power circuit into the low-voltage control systems.**

Manuscript received January 24, 2017; revised April 12, 2018; accepted May 21, 2018. Date of publication May 31, 2018; date of current version December 7, 2018. This work was supported by the Natural Sciences and Engineering Research Council and the Canada Research Chair Program. Recommended for publication by Associate Editor K. Ngo. *(Corresponding author: Matthew M. Wilkins.)*

M. M. Wilkins is with the Department of Physics and the School of Electrical and Computer Engineering, University of Ottawa, Ottawa, ON K1N6N5, Canada (e-mail:

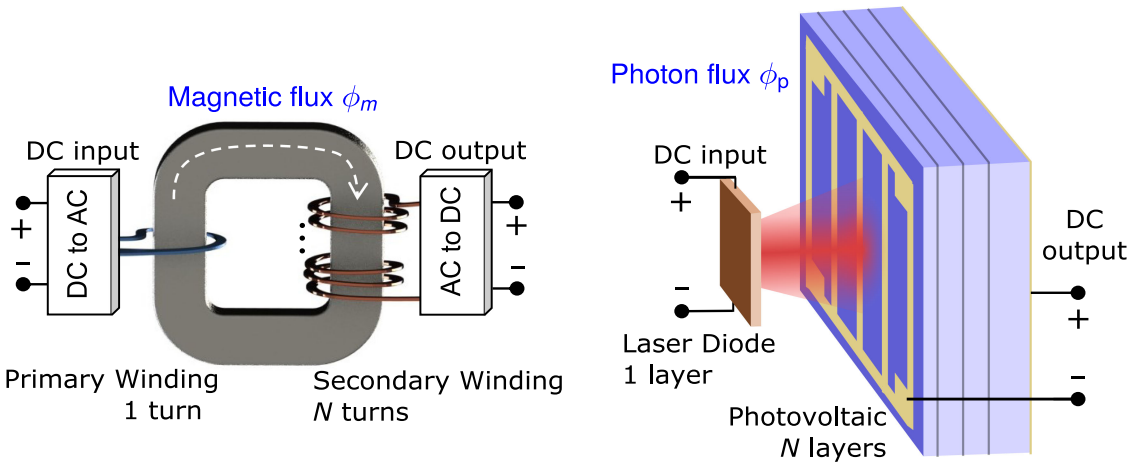

(a) (b)

Fig. 1. Isolated N-times voltage conversion using (a) magnetic (i.e., transformer) and (b) photonic technologies.

cases, this has been done by segmenting a single planar junction into pie-shaped mesas, which are isolated and connected in series via microfabrication [19]–[21]. More recently, vertically stacked PPCs with a structure similar to that of multijunction solar cells have been demonstrated with 2 [22], [23], 5, 12, and 20 junctions [3], [24], as in Fig. 1(b). The segmented planar design fundamentally requires a design tradeoff between resistivity of the series connecting conductors and the amount of device area, which is shaded by these elements [22]. The vertical design, which employs optically transparent tunnel diodes for series connection of the photovoltaic junctions, requires no such tradeoff and the elimination of isolation trenches and series connecting elements yields a smaller device area. Consequently, this vertical structure enables higher conversion efficiencies and higher power densities [22], with output voltages proportional to the number of stacked n-p junctions, having demonstrated up to 23 V to date. When coupled to a laser diode, the result is a circuit that provides dc–dc boost conversion without the need to convert to ac as an intermediate step. Although the efficiency of this approach is not as high as in a conventional switching boost converter, the advantages include reductions in complexity, volume and parts count, and the elimination of ripple associated with switching boost converters.

Table I provides a relative comparison of switching and photonic conversion on several metrics. Photonic conversion has excellent isolation, since it is possible to provide a larger separation distance between laser and PPC to realize an arbitrarily large electrical isolation while keeping the same efficiency. Both photonic and switching technologies are highly scalable, as it is possible to fabricate the devices to the required size or assemble several devices for a given application. The market for PPCs using this architecture is not established at this time, so cost of the photonic technology is expected to change as the market develops. The photonic assemblies use III-V based semiconductor devices, which are more expensive than silicon, but this higher cost will be partially offset by a reduced parts count. The remaining metrics in Table I are discussed in the following sections.

TABLE I
QUALITATIVE COMPARISON OF PHOTONIC AND MAGNETIC POWER CONVERSION

	Switching	Photonic
Power Density	Excellent	Good
Efficiency	Excellent	Fair
Isolation	Fair	Excellent
Scalability	Excellent	Excellent
Expected Cost	Excellent	Good
Ripple	Fair	Excellent
EMI rejection	Good	Excellent

To our knowledge, this is the first reported result for system efficiency of such a laser/PPC system with >12 V output capability. Given that the PPCs used here are roughly twice as efficient as previous generations, we believe that this system efficiency is greater than has been achieved before and sets a benchmark for future improvements through new laser sources, optical system design, and thermal management.

The paper is structured as follows. In Section II, we describe the optical characteristics and power conversion efficiency of the coupled laser and PPC device. We then apply it, first to a dc–dc boost converter with minimal ripple in Section III, and then in a switching circuit requiring a dc supply with minimal capacitive coupling to ground in Section IV.

II. COUPLING OF LASER AND PPC

The laser used is a commercially available 1 mm × 0.8 mm vertical-cavity surface-emitting laser (VCSEL) array with 202 laser elements [see Fig. 2(a)]. The array emits nominally 1 W at 850 nm. The current- and temperature-dependence of the

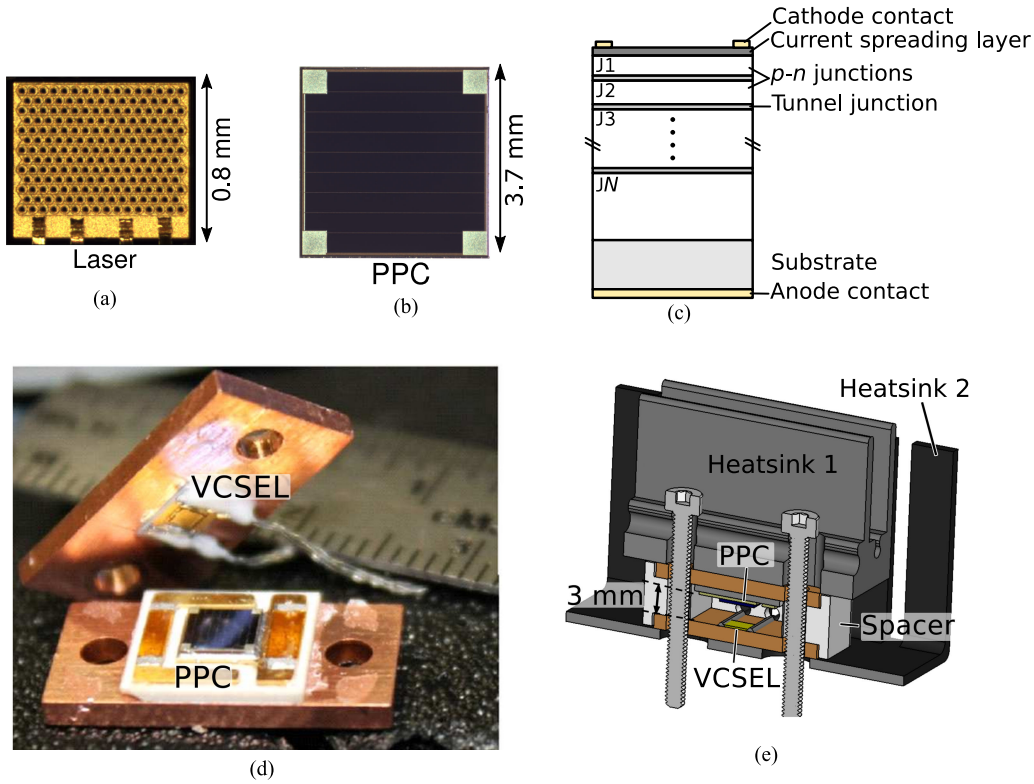

Fig. 2. VCSEL laser array and PPC devices. (a) Microscope image of the laser diode chip. (b) Microscope image of the PPC chip. (c) Layer structure of the PPC showing the multiple series-connected p-n junctions. (d) VCSEL array and PPC on copper carriers. (e) Cutaway view of the VCSEL array and PPC, with a plastic spacer providing galvanic isolation. The laser array and PPC are each connected to separate, electrically isolated heatsinks. Plastic screws serve to hold the assembly together and mount it to a PCB (not shown).

emission peak is in Fig. 3(a). The peak wavelength shifts by 1.4 nm/A and 0.08 nm/°C. The PPCs are 3.7 mm × 3.7 mm and are designed and manufactured by Azastra Opto Inc. (acquired by Broadcom Semiconductors ULC) based on the vertical epitaxial heterostructure architecture (VEHSA). The structure contains 12 GaAs series-connected n-p junctions of varying thickness, grown by metal-organic chemical vapor deposition on a GaAs substrate. Each junction generates ∼1.15 V at open circuit, so that the open-circuit voltage of the entire PPC is >14 V. A microscope image of the PPC chip is shown in Fig. 2(b), and a cross-sectional view of the layer structure is in Fig. 2(c). A two-layer dielectric antireflective coating tuned to the laser wavelength is applied to the PPC.

The VCSEL laser diode array and the PPC are packaged on separate copper submounts [see Fig. 2(d)]. We orient the two devices facing one another with a 3-mm airgap, which is maintained by a plastic spacer, providing an isolation voltage >1 kV. The two submounts are passively cooled with separate aluminum heatsinks [see Fig. 2(e)], which are also separated by an airgap.

Since the absorption coefficient of GaAs is wavelength dependent, PPCs with the vertical architecture must be designed for optimal operation at a specific wavelength. Photocurrent is generated equally in each of the N series-connected junctions through a careful choice of layer thicknesses. Each optically thin junction is designed to absorb $(1-T)/N$ of the incident light, where T is the fraction of light transmitted through all junctions without being absorbed. The total absorber thickness for the PPC design used herein was 3.5 μm, so that T is less than 1%. The design rules for the choice of individual layer thicknesses are outlined in [25]. The spectral response of the PPC is characterized by its internal quantum efficiency (IQE), which is the ratio of electron flux across the device terminals to absorbed photon flux. IQE for $N = 12$ PPC was measured using a Newport IQE-200 system, and is shown in Fig. 3(b). Whereas multijunction solar cells are usually light-biased to produce a measure of the quantum efficiency of an individual junction, all of the junctions of the PPC absorb over the same range of wavelengths and so light-biasing is not possible. Instead, we measure the IQE of the entire device under single-wavelength illumination, without light biasing.

We might expect that this wavelength sensitivity would increase for increasing N, however experiments have shown essentially no change in wavelength response for 5, 6, 12 or 20-junction devices [1]. This is explained through the phenomenon of luminescent coupling (LC) [26]–[28], where one junction is absorbing more than its share of incident photons, the excess is re-emitted as photons with energy near the material bandgap. These photons are reabsorbed in the other junctions, leading to an efficient redistribution of photocurrent between the junctions [29]–[31].

The impact of this LC has been evaluated through device simulations. Simulated IQE results were calculated using a drift-diffusion based solver as described in [29], and an overview of

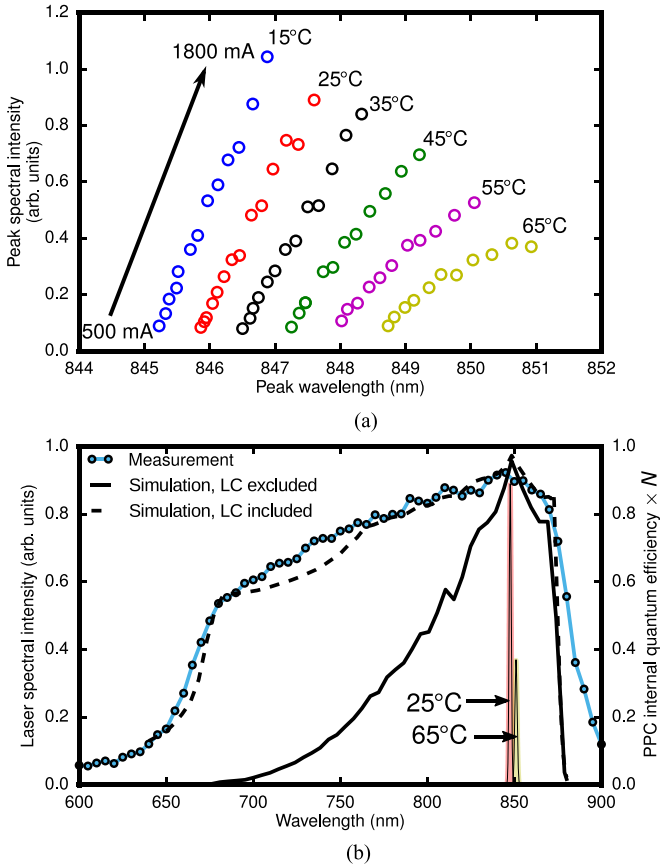

Fig. 3. Wavelength-matching of the laser diode and PPC. (a) Laser wavelength and peak intensity for varying temperature and applied current. (b) Measured IQE of the $N = 12$ junction PPC (blue dots), compared to simulations including (dashed) and excluding (solid) the effects of LC. Measured laser emission spectra are shown at two temperatures.

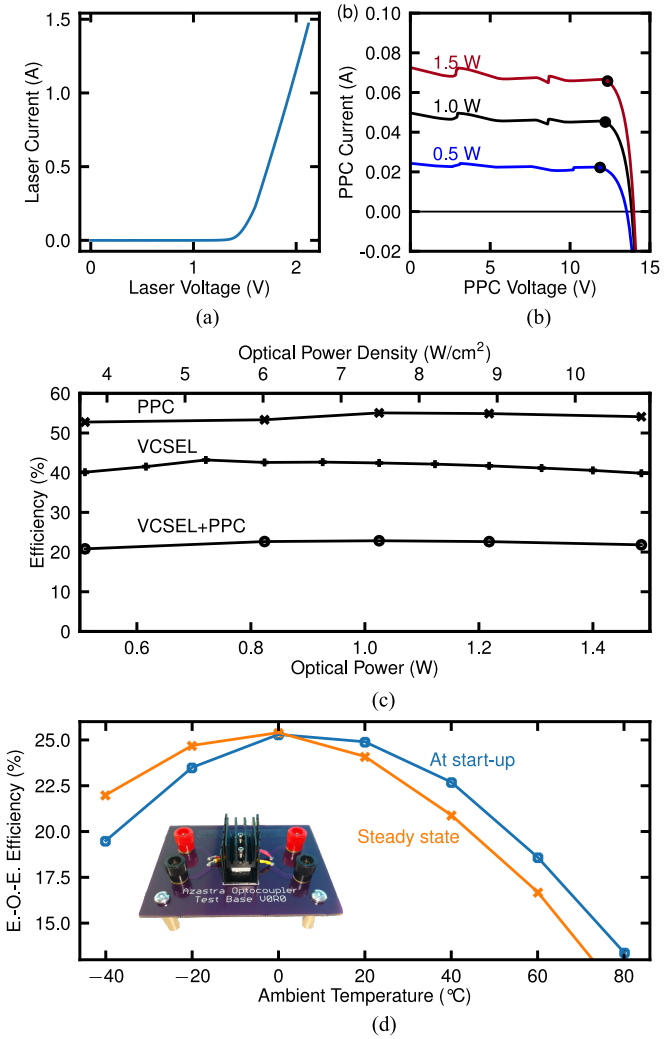

Fig. 4. Terminal characteristics of the optically isolated dc power supply. (a) Current-voltage characteristics for the VCSEL laser diode array at 25 °C. (b) Current-voltage characteristics for the PPC at the same temperature for illumination of 0.5, 1, and 1.5 W. (c) Efficiency of the VCSEL laser, the PPC, and the complete power converter as a function of optical power and optical power density on the bottom and top axes, respectively. (d) Overall E.-O.-E. power conversion efficiency of the coupled device, operating at 1-W optical power, with each data point taken immediately at start-up from a cold condition and after reaching a steady-state temperature. Inset: image of the coupled laser/PPC package.

our process for device simulations is found in [32]. This redistribution of light and resultant photogeneration yields a broadened IQE, shown for a 12-junction PPC in Fig. 3(b). With LC excluded from the simulation, the device short-circuit current is limited by the n-p junction with the lowest photocurrent, leading to a strong sensitivity to wavelength (-1.1%/nm) near the design point of 850 nm. When the effects of LC are included, this sensitivity is reduced to -0.4%/nm and closely follows experiment. In Fig. 3(b), we also show measured spectra of a laser diode array at temperatures of 25 °C and 65 °C. Although the laser wavelength is nominally well-matched to the PPC, the small shift in wavelength as a function of current and temperature can be significant. Consequently, nearly three-fold reduction in wavelength sensitivity due to LC is important to maintain high efficiency of operation without temperature stabilization of either the laser or the PPC.

The laser and the PPC are separated by an airgap of 3 mm, and are coupled such that >99% of light emitted by the laser is incident on the PPC. The overall electrical-to-optical-to-electrical efficiency (E.-O.-E.) η_{eoe} of the power converter is the product of the laser efficiency η_{laser}, the optical coupling efficiency η_{optical}, and the PPC efficiency η_{PPC}

$$\eta_{\mathrm{eoe}} = \eta_{\mathrm{laser}}\,\eta_{\mathrm{optical}}\,\eta_{\mathrm{PPC}}. \tag{1}$$

The operating principle of the converter can be understood by studying the current-voltage characteristics of the laser and the PPC, as shown in Fig. 4(a) and (b), respectively. The laser diode emits with a peak electrical-to-optical efficiency of 42%. Optical power output from the laser increases linearly with current, according to

$$P_{\mathrm{opt}} = \frac{hc}{q\lambda}\eta_{\mathrm{ext}}(I - I_{\mathrm{th}}) \tag{2}$$

where h is Planck's constant, c is the speed of light, λ is the laser wavelength, η_{ext} is the laser's differential external quantum efficiency (efficiency of converting electrical current into emitted photons), and I_{th} is the laser's threshold current, 300 mA in this case [33].

The PPC used here has 12 GaAs junctions and provides a voltage of 14.5 V under open-circuit conditions and 12.4 V at maximum power. Each junction behaves as an ideal diode

$$V_i = \frac{\gamma_i kT}{q} \ln\left(\frac{I_{\mathrm{ph},i} - I}{I_{0,i}}\right) \tag{3}$$

where i indexes the junctions, γ_i is the ideality factor of an individual diode junction, $I_{\mathrm{ph},i}$ is the photogenerated current, $I_{0,i}$ is the saturation current density, and I is the current density conducted through the full device [34]. Assuming that the incident optical power is shared equally in each of the junctions, the photocurrent density in each junction is

$$I_{\mathrm{ph},i} = \frac{q\,\eta_{\mathrm{optical}} P_{\mathrm{opt}}}{N} \frac{\lambda}{hc}. \tag{4}$$

If all junctions have the same ideality factor γ and saturation current I_0, the voltage across all N series-connected junctions is then

$$V = \sum_{i=1}^{N} V_i = \frac{N\gamma kT}{q} \ln\left(\frac{I_{\mathrm{ph}} - I}{I_0}\right). \tag{5}$$

The power output of the PPC varies with voltage, and so output is maximized when it is connected to a properly matched load, either by design or by active control of the converter [35]. In practice, the amount of light absorbed in each of the junctions is not equal, and so the measured current-voltage curves in Fig. 4(b) show some deviations from the ideal behavior of (5). A more sophisticated analytical model for tandem multijunction devices, which incorporates the effects of LC is outlined in [36]. The short-circuit current of the PPC is proportional to input optical power, as shown in Fig. 4(b). At 25 °C, optical-to-electrical power conversion efficiency η_{PPC} is 55% with 1 W of optical power, and is >50% over a wide range of optical power up to at least 11 W/cm^2, which was the maximum intensity applied [see Fig. 4(c)].

When combined, the laser diode array and PPC provide a step-up in voltage from 2.5 to 14 V. The laser can be operated at dc, producing no high-frequency switching and hence no internally generated EMI. Alternatively, it can be regulated in a pulse mode such that it operates at its maximum efficiency independent of the load at the output. Overall the coupled laser/PPC pair has an efficiency of 23% at 25 °C. When the ambient temperature is varied [see Fig. 4(d)], we find a peak in efficiency of 25% at ∼10 °C. To our knowledge, this is the first published result for efficiency of such a coupled device. The peak shifts to 0 °C if the device is allowed to warm up to the temperature before taking the efficiency measurement, indicating approximately a 10 °C rise in junction temperature from startup to steady state.

While the 23% overall conversion efficiency is considerably less than comparable linear or switch-mode power supplies, future development of the laser and PPC specifically for this application provides a significant potential for improvement. The laser used in this study is 42% efficient at room temperature, but the literature reports high power laser diodes up to 76% efficiency at a wavelength of 973 nm [37], which would permit an 80% relative increase in overall efficiency if a PPC matched to the 973-nm wavelength can be developed. High-power LED light sources with 85% efficiency sustained over the temperature range of 25 to 80 °C [38] could yield an even larger increase in efficiency and broader operating temperature range.

On the optical-to-electrical conversion side, the particular PPC devices used in this study were up to 55% efficient, but similar 5-junction, 6-V devices have recently shown up to 70% conversion efficiency (a 27% relative increase) [24]. There are engineering methods to improve this efficiency further, by careful optical design of the PPC. The well-known Shockley-Queisser limit for solar cells, which is based on a detailed balance analysis of optical absorption and emissions from device, provides a limiting efficiency of 33% for a solar cell with the optimum bandgap and illuminated by the terrestrial solar spectrum [39], [40]. This analysis, however, is based on the necessity to collect energy from the sun, which is a broadband, blackbody source of finite temperature. Green demonstrated that a similar analysis of an ideal photovoltaic device absorbing monochromatic light yields a limiting efficiency of 100%, as the spectral and angular distribution of the incoming light can be arbitrarily narrow, and the intensity can be arbitrarily high [41]. Similarly, Green found that the limiting Carnot efficiency of a monochromatic laser-PPC system tends to 100% as the intensity of the laser increases.

Under normal conditions, the output current of the PPC is proportional to the incident light intensity, but is ultimately limited by the peak tunneling current density of the tunnel junctions, which are used to make ohmic connections between adjacent p-n junctions. Tunnel junctions of this type have been demonstrated with peak current densities over 6×10^3 A/cm^2 [42], which corresponds to an optical intensity of 9 kW/cm^2 per junction at the wavelength of 830 nm. To date, PPCs have been demonstrated with a real power density up to 100 W/cm^2 [22], while VCSEL laser arrays and edge-emitting laser arrays can support continuous power densities >1 kW/cm^2[43].

In the demonstrations presented here, the laser and PPC are connected to separate, passively air-cooled heatsinks. These heatsinks rise 11 K/W, limiting the laser to approximately 4.5-W continuous optical output power. This yields 2.45-W electrical output from the PPC, for a power density of 0.2 W/cm^3. For comparison, current switch-mode devices optimized for power density have ∼1 W/cm^3, and the U.S. Department of Energy has proposed a power density target of 16.4 W/cm^3 [44]. In future developments, using commercially available liquid-cooled laser modules [45] and a similar cooling strategy for the PPC, could yield a power density of 15 W/cm^3, based on a system volume that includes the semiconductor/liquid heat exchangers but not the associated pump and liquid/air heat exchanger.

III. Ripple-Free Boost Converter

Step-down dc–dc voltage converters are well-established using both linear and switching designs. Step-up (boost) dc–dc voltage converters, on the other hand, are possible only when using switching approaches presently. Conventional technology for step-up dc–dc conversion requires a "boost converter" circuit where a voltage is applied to an inductor to establish current, and the current is then switched to charge a capacitor. This leads

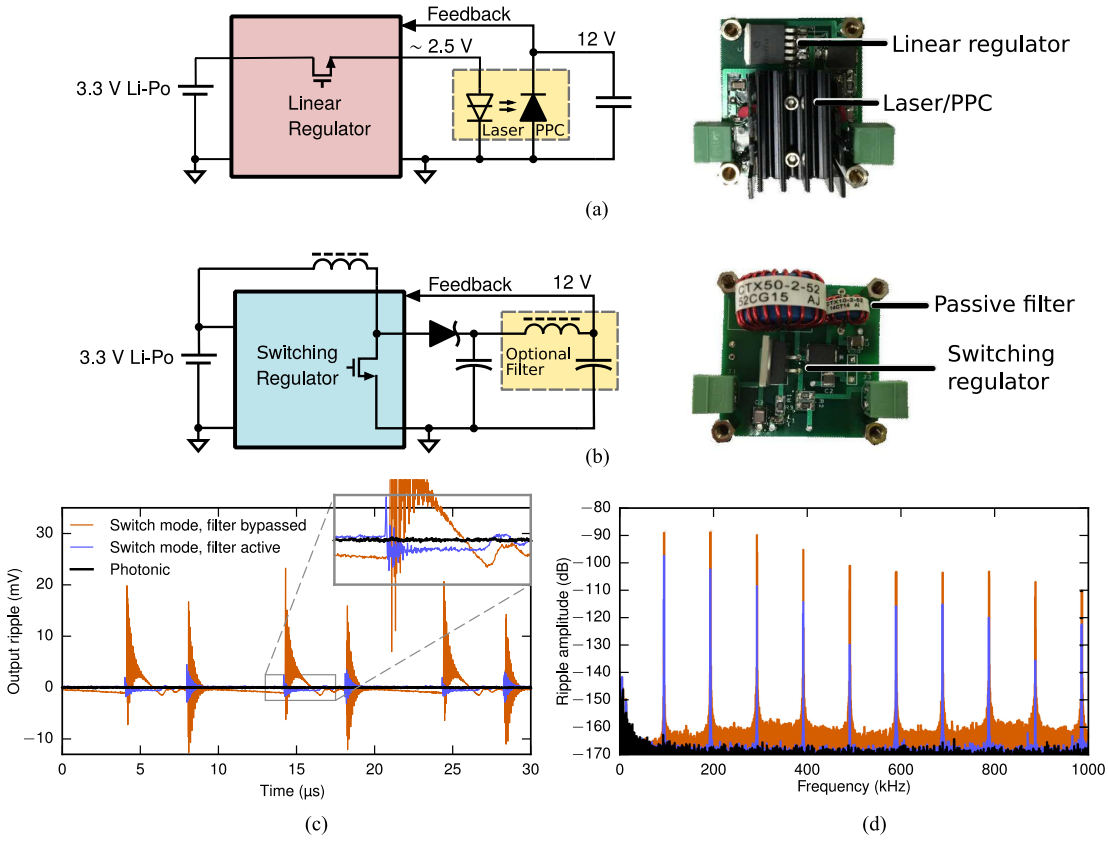

Fig. 5. Performance of regulated boost converters. (a) Photonic boost converter topology. (b) Conventional switching boost converter topology with optional *LC* filter at the output. (c) Ripple of the switching and photonic boost converters in the time domain. (d) Frequency-domain representation of the same data, referenced to the 12-V dc output voltage. The noise floor is higher in the orange data set because a different gain setting was required.

to a characteristic ripple in the output voltage as the regulator switches ON and OFF. Additionally, there is a ringing of the circuit at its resonant frequency, forced by the switching impulses.

Using our alternative photonics-based technology, a diode laser was coupled to a 12-V PPC and connected to the output of a linear regulator to produce a step-up converter [see Fig. 5(a)] that is free of ripple, ringing, and EMI emissions. Thus, the system converts the voltage commonly available from a single lithium polymer (Li-Po) battery cell (3.0 to 3.7 V) to a regulated 12 V output. The circuit uses a RichTek RT9183 linear regulator, with feedback from the 12 V output of the PPC.

As our baseline for comparison, we assembled a switching boost converter [see Fig. 5(b)], based on a Linear Technologies LT1171 regulator. Switching frequency is 100 kHz. The circuit includes an output *LC* filter with a cutoff frequency of 5 kHz.

Measurements were made with an Agilent 6014A oscilloscope at 2×10^9 samples/s, with boxcar averaging for improved vertical resolution. Some specific frequencies were identified, which were present at consistent levels in all circuit configurations, as well as in a reference measurement taken with the boost converter powered OFF. These noise sources are therefore internal to the oscilloscope or supporting equipment and the corresponding frequencies are removed from Fig. 5(d) for clarity.

Noise and ripple of the photonic and switching circuits in the time and frequency domains are shown in Fig. 5(c) and (d), respectively. When the *LC* filter is bypassed in the switching circuit, we measure a root-mean-square (rms) ripple of 2.48 mV (35.9 mV peak to peak). The ripple is reduced to 0.49 mV rms (7.76 mV peak to peak) with the *LC* filter active. In the frequency domain [see Fig. 5(d)], the switching circuit produces harmonics at multiples of the switching frequency, 100 kHz.

In contrast, the photonic boost converter shows no significant frequency content over the 50 kHz–20 MHz range. With no load, it draws 280 mA, which is just below the lasing threshold; with a 330-Ω resistive load the current draw is 986 mA. Using an oscilloscope sampling at 2×10^9 samples/s and limited to 20 MHz analog bandwidth, we were unable to detect any ripple above the 0.33 mV peak-peak (0.045 mV rms) background noise of our instrument. The 0.045-mV rms ripple for the photonic boost converter represents a 98.1% reduction relative to the switched, filter-less design. These results are tabulated in Table II. Under continuous operation, the heatsinks for the laser and the PPC rose to 53 and 54 °C, respectively.

IV. Optically Isolated Gate Drive Power Supply

Next, we consider a second application in power electronics. Wide bandgap transistors, and particularly SiC metal-oxide-semiconductor field-effect transistors (MOSFETs), are increasingly available and are being integrated into power electronics systems [46]–[50]. The small gate capacitance and the majority-

TABLE II
POWER DRAW AND OUTPUT RIPPLE OF THE TWO BOOST CONVERTER DESIGNS

	Power Draw (W)		Efficiency (%)	Volume (cm^3)	Power Density (W cm^{-3})	Ripple (mV)	
	No load	With load				RMS	p-p
Switching, filter bypassed	0.044	0.56	77.6	17.6	1.7	2.48	35.9
Switching, filter active	0.044	0.56	77.6	20.0	1.5	0.49	7.76
Photonic	0.92	3.4	12.7	13.6	0.2	<0.045	<0.33

Ripple was measured with a 330-Ω (435 mW) resistive load. Operating temperature of the PPC was 54 °C under continuous operation.

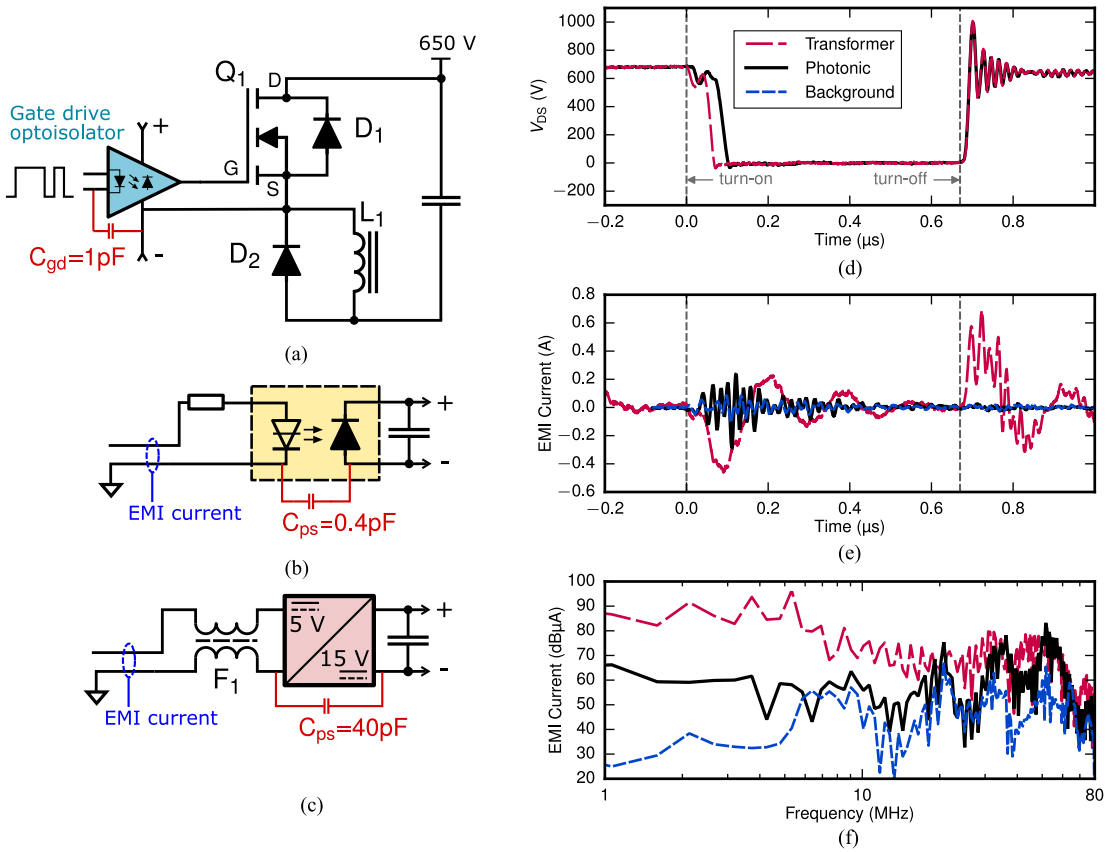

Fig. 6. Double-pulse switching circuit used to test the effects of different gate drive power supplies. (a) SiC MOSFET, load inductor, and gate driver. Parasitic capacitances, which provide a path for EMI currents are shown in red. (b) Optically isolated system, which provides a floating power supply for the gate drive optoisolator. (c) Conventional dc–dc converter with transformer isolation and common-mode filter. (d) Switching waveforms using conventional and optically isolated gate power supplies. (e) Measured EMI currents through the transformer-based and photonic power supplies. A reference measurement with the current probe disconnected is also shown. (f) Frequency-domain representation of the EMI current.

carrier nature of SiC MOSFETs promises fast switching times and reduced switching losses when compared with established technology based on silicon transistors. These increases in switching speed come with increased EMI and instability of the power electronic system [51]. The power supplies to the high-side gate drivers in an H-bridge or a three-leg converter typically are isolated using transformers, which have a significant stray capacitance and offer a path for conducted EMI. To investigate the impact of a photonic power supply to the gate driver on switching performance and EMI, we used a double-pulse test setup [51]–[53] [see Fig. 6(a)], with the gate drive signal optoisolator powered using either a PPC or a conventional dc–dc converter (see Fig. 6(b) and (c), respectively). Details of the test setup and components can be found in [54]. In the photonic implementation, a VCSEL laser diode array, which is referenced to electrical ground, is used to illuminate a PPC, which supplies power to the high-side gate driver. As described in Section II, in continuous operation, the output of the photonic converter is limited to 2.45 W, due to temperature rise of the laser.

The setup simulates one of the high-side switching devices in a three-leg power converter, comparable to what is used in

hybrid-electric vehicle drive systems. We establish a 90-A current in the load inductor L_1 and then measure waveforms during a single OFF/ON pulse lasting 0.67 μs. As Q_1 is switched OFF, the inductor current freewheels through the diode D_2. The MOSFET Q_1 is a Cree SiC device with breakdown voltage of 1200 V and maximum current of 120 A. Q_1 is controlled by an optoisolated gate driver with a CMOS totem pole output stage. The optoisolator, in turn, requires an isolated power supply of >13 V. No gate resistors are used to limit the switching slew rate, which is desirable for high efficiency in power electronic circuits but leads to harsh switching transients and potential problems with EMI. Although we have only tested the system in the double-pulse mode, we can estimate the average power required for continuous operation based on the energy required to charge the gate capacitance $C_{\rm iss}$ of the SiC MOSFET

$$P_{\rm sw} = C_{\rm iss} V_{\rm gs}^2 f_{\rm sw} \tag{6}$$

where $C_{\rm iss} = 2800$ pF, the on-state gate-source voltage $V_{\rm gs} = 12$, and switching frequency $F_{\rm sw} = 100$ kHz. We calculate $P_{\rm sw} = 40$ mW, so the photonic power supply, which has a maximum output power of 2.45 W (0.22 A) is capable of driving the circuit in steady state. With a rise time of 10 ns, the gate drive current has transient pulses of 1.6 A. For this reason, a 2 μF high-frequency multilayer ceramic capacitor is used to buffer the output of the photonic converter.

When Q_1 switches as in Fig. 6(d), its source and drain terminals undergo rapid changes in potential. The output sides of the gate drive optoisolator and its power supply are also subjected to these potential swings. Both devices have a finite capacitance between the input and output of the gate driver ($C_{\rm gd}$) and its power supply ($C_{\rm ps}$), and so any switching event must lead to a common-mode EMI current, $i_{\rm CM}$, from the outputs back to the low-voltage control circuitry at the inputs

$$i_{\rm CM} = (C_{\rm gd} + C_{\rm ps})\, dV/dt. \tag{7}$$

For the photonic power supply, the stray capacitance between laser and PPC chips is only 60 fF; the capacitance between heatsinks on the laser and PPC sides is larger for a total $C_{\rm ps} = 0.4$ pF. This could be reduced significantly with suitable redesign of the packaging, which had not been optimized for this performance metric.

As a benchmark, we also tested a more conventional supply with a transformer-based dc–dc converter [see Fig. 6(c)], based on the Delta SA01S0515A dc–dc converter. For supply voltages $V_{\rm DC} > 75$ V, the stray capacitance of this device is sufficient to cause the SiC MOSFET to fail to turn OFF because the gate potential cannot rise quickly enough to maintain a positive potential relative to the source terminal. This is addressed by adding a common-mode filter F1 with 200-Ω impedance to common-mode currents at 1 MHz. The filter F1 is used in all measurements presented here, and enables the system to switch correctly at $V_{\rm DC}$ up to 650 V. This solution has a 100-times larger capacitance $C_{\rm ps}$ of 40 pF, due to the primary and secondary windings of the transformer being wound in close proximity on a magnetic core.

Switching response is shown in Fig. 6(d)–(f). The drain-source voltage across the SiC MOSFET, $V_{\rm DS}$ is plotted in Fig. 6(d). Large switching transients are produced at turn-off and settled out after 0.1 μs. The turn-on of the MOSFET powered by the photonic converter is delayed 30 ns relative to the transformer-based reference. This is because the photonic converter provides a voltage of 13.5 V, determined by the open-circuit voltage of the PPC, while the transformer-based circuits provides 15 V and is able to charge the gate capacitance more quickly. There is no such delay in the turn-off at 0.6 μs, where both systems are driving the gate voltage to zero. This turn-on delay could be addressed by adapting the PPC design to use 14 junctions rather than 12.

In Fig. 6(e), we show a common-mode EMI current measured on the power supply cable leading to the digital control electronics, which generate switching signals for the MOSFET. With the transformer-based power supply including common-mode filter F1, the EMI current magnitude reaches a peak of 0.64 A, while the photonic circuit reaches 0.25 A peak. A third measurement with the current probe removed from the wires shows a peak of 0.1 A, indicating that the measurements are partly obscured by EMI picked up directly by the instrument. However, the background signal is consistent, and smaller than either of the EMI current measurements. A frequency analysis of the EMI currents is shown in Fig. 6(f). The photonic-based gate drive power supply reduces EMI current by 20 to 30 dB over the 0 to 10 MHz range. The largest peak in the EMI from the transformer-based power supply, 96 dBμA at 5.3 MHz, is reduced by 38 dB with the photonic power supply (a factor of 80 reduction). With both the transformer-based and photonic power supplies, we find peaks at 45 and 65 MHz; these peaks are largely unaffected by the choice of power supply and may be coupled through the optoisolator, $C_{\rm gd}$. Hence the gate drive power supply capacitance $C_{\rm ps}$ is no longer the most significant path for conducted EMI in the photonic configuration. The proposed photonic-based gate drive power supply is a unique solution offering high impedance to EMI without large passive components, and consequently has benefits in terms of parts count. With sufficient spatial separation between the laser and the PPC, transient voltage stress can be minimized, and this low stress combined with the low parts count should yield high reliability.

V. Conclusion

PPCs enable the creation of a unique class of step-up voltage converters, which have practical output voltage in the range of 5, 12, or 24 V while causing no ripple, ringing or EMI. Output voltage of 48 V dc or more from a monolithic PPC may be achievable in the future [1]. While the overall efficiency $\eta_{\rm eoe} = 23\%$ demonstrated here is lower than existing linear or switching power converters, using present technology has already shown light sources with nearly double the efficiency and PPCs with 27% (relative) higher efficiency than the devices used herein. Furthermore, there is no fundamental (thermodynamic) barrier to improving the PPC efficiency, $\eta_{\rm PPC}$ further. These improvements would make the system competitive with linear technologies, and possibly some switching technologies, in terms of power conversion efficiency.

In this paper, we have demonstrated two new applications of this technology. First, the *photonic boost converter* achieves direct dc–dc conversion without an intermediate ac stage. When compared with a switching boost converter, this circuit eliminates the introduction of additional harmonics or ripple, and our measurements demonstrate no signal above the noise floor, which is 60 to 80 dB below the harmonics of the boost converter over a broad frequency range. Second, the *optically isolated dc supply* reduces EMI conducted to the signal-level electronics, and is applicable to electric vehicle applications. It provides a 20 dB improvement, over a magnetically isolated supply, again limited primarily by measurement noise. While the devices discussed here were intended to be compact integrated solutions, the same or improved functionality can be realized using larger gaps with free-space separations or the introduction of optical fibre for a range of centimeters to kilometers of separation. With large separation, the capacitive coupling $C_{\rm ps}$ can be made arbitrarily small and the breakdown voltage can be made large without compromising the optical coupling efficiency $\eta_{\rm optical}$. This makes the photonic converter useful in systems operating at 10 kV or greater. These emerging applications leverage the significant advances in laser diode and multijunction solar cell technology developed in recent years [55], and reveal potential new markets for photonic devices.

REFERENCES

[1] S. Fafard *et al.*, "High-photovoltage GaAs vertical epitaxial monolithic heterostructures with 20 thin p/n junctions and a conversion efficiency of 60%," *Appl. Physics Lett.*, vol. 109, no. 13, 2016, Art. no. 131107. [Online]. Available: http://scitation.aip.org/content/aip/journal/apl/109/13/10.1063/1.49641 20

[2] C. E. Valdivia *et al.*, "Five-volt vertically-stacked, single-cell GaAs photonic power converter," in *Proc. SPIE*, 2015, vol. 9358, pp. 93580E-1–93580E-8. [Online]. Available: http://proceedings.spiedigitallibrary.org/proceeding.aspx?doi=10.1117/1 2.2079824

[3] S. Fafard *et al.*, "Ultrahigh efficiencies in vertical epitaxial heterostructure architectures," *Appl. Phys. Lett.*, vol. 108, no. 7, 2016, Art. no. 071101. [Online]. Available: http://scitation.aip.org/content/aip/journal/apl/108/7/10.1063/1.4941240 http://aip.scitation.org/doi/10.1063/1.4941240

[4] B. J. Baliga, "The future of power semiconductor device technology," *Proc. IEEE*, vol. 89, no. 6, pp. 822–832, Jun. 2001.

[5] J. Kassakian, "Automotive electrical systems-the power electronics market of the future," in *Proc. 15th Annu. IEEE Appl. Power Electron. Conf. Expo.*, 2000, pp. 3–9.

[6] M. Enohnyaket and J. Ekman, "Analysis of air-core reactors from DC to very high frequencies using PEEC models," *IEEE Trans. Power Del.*, vol. 24, no. 2, pp. 719–729, Apr. 2009.

[7] J. M. Rivas, O. Leitermann, Y. Han, and D. J. Perreault, "A very high frequency dc-dc converter based on a class (Φ_2) resonant inverter," *IEEE Trans. Power Electron.*, vol. 26, no. 10, pp. 2980–2992, Oct. 2011.

[8] M. Xu, Y. Ren, J. Zhou, and F. C. Lee, "1-MHz self-driven ZVS full-bridge converter for 48-V power pod and dc/dc brick," *IEEE Trans. Power Electron.*, vol. 20, no. 5, pp. 997–1006, Sep. 2005.

[9] Y. Ren, M. Xu, C.-S. Leu, and F. C. Lee, "A family of high power density unregulated bus converters," *IEEE Trans. Power Electron.*, vol. 20, no. 5, pp. 1045–1054, Sep. 2005.

[10] M. Tsukuda, I. Omura, W. Saito, and T. Domon, "Demonstration of high output power density (50 W/cc) converter using 600 V SJ-MOSFET and SiC-SBD," in *Integrated Power Systems (CIPS)*, H. J. Levinson and M. V. Dusa, Eds. Naples, Italy: VDE, 2006.

[11] D. Han and B. Sarlioglu, "Study of the switching performance and EMI signature of SiC MOSFETs under the influence of parasitic inductance in an automotive dc–dc converter," in *Proc. IEEE Trans. Electrific. Conf. Expo.*, 2015, pp. 1–8. [Online]. Available: http://ieeexplore.ieee.org/document/7165824/

[12] N. Oswald, P. Anthony, N. McNeill, and B. H. Stark, "An experimental investigation of the tradeoff between switching losses and EMI generation with hard-switched All-Si, Si-SiC, and All-SiC device combinations," *IEEE Trans. Power Electron.*, vol. 29, no. 5, pp. 2393–2407, May 2014. [Online]. Available: http://ieeexplore.ieee.org/document/6582542/

[13] A. Goldberg, J. Kassakian, and M. Schlecht, "Issues related to 1–10-MHz transformer design," *IEEE Trans. Power Electron.*, vol. 4, no. 1, pp. 113–123, Jan. 1989. [Online]. Available: http://ieeexplore.ieee.org/document/21880/http://ieeexplore.ieee.org/document/7077205/

[14] P. Tenant and J. Rousseau, "Dynamic model of magnetic materials applied on soft ferrites," *IEEE Trans. Power Electron.*, vol. 13, no. 2, pp. 372–379, Mar. 1998. [Online]. Available: http://ieeexplore.ieee.org/document/662859/

[15] Hai Yan Lu, Jian Guo Zhu, and S. Hui, "Experimental determination of stray capacitances in high frequency transformers," *IEEE Trans. Power Electron.*, vol. 18, no. 5, pp. 1105–1112, Sep. 2003. [Online]. Available: http://ieeexplore.ieee.org/document/1224466/

[16] A. Chub, D. Vinnikov, F. Blaabjerg, and F. Z. Peng, "A review of galvanically isolated impedance-source DC-DC converters," *IEEE Trans. Power Electron.*, vol. 31, no. 4, pp. 2808–2828, Apr. 2016. [Online]. Available: http://ieeexplore.ieee.org/document/7151820/

[17] H. Fujita and M. Ishigaki, "A resonant gate-drive circuit with optically-isolated control signal and power supply for fast-switching and high-voltage power semiconductor devices," in *Proc. Int. Power Electron. Conf.*, 2010, pp. 1895–1901. [Online]. Available: http://ieeexplore.ieee.org/document/5542024/

[18] J. Levinson *et al.*, "Towards fully autonomous driving: Systems and algorithms," in *Proc. IEEE Intell. Veh. Symp.*, 2011, pp. 163–168. [Online]. Available: http://ieeexplore.ieee.org/document/5940562/

[19] R. Peña, C. Algora, and I. Anton, "GaAs multiple photovoltaic converters with an efficiency of 45% for monochromatic illumination," in *Proc. IEEE 3rd World Conf. Photovolt. Energy Convers.*, Osaka, Japan, 2003, pp. 228–231.

[20] R. Peña and C. Algora, "One-watt fiber-based power-by-light system for satellite applications," *Progress Photovolt.: Res. Appl.*, vol. 20, no. 1, pp. 117–123, 2012. [Online]. Available: http://doi.wiley.com/10.1002/pip.1130

[21] L. Wagner, A. W. Bett, and H. Helmers, "On the alignment tolerance of photovoltaic laser power converters," *Optik—Int. J. Light Electron Optics*, vol. 131, pp. 287–291, 2017. [Online]. Available: http://linkinghub.elsevier.com/retrieve/pii/S0030402616313985

[22] J. Schubert, E. Oliva, F. Dimroth, W. Guter, R. Loeckenhoff, and A. W. Bett, "High-voltage GaAs photovoltaic laser power converters," *IEEE Trans. Electron Devices*, vol. 56, no. 2, pp. 170–175, Feb. 2009.

[23] S. K. Reichmuth, H. Helmers, S. P. Philipps, M. Schachtner, G. Siefer, and A. W. Bett, "On the temperature dependence of dual-junction laser power converters," *Progress Photovolt.: Res. Appl.*, vol. 25, no. 1, pp. 67–75, 2017. [Online]. Available: http://doi.wiley.com/10.1002/pip.2814

[24] S. Fafard *et al.*, "Advances with vertical epitaxial heterostructure architecture (VEHSA) phototransducers for optical to electrical power conversion efficiencies exceeding 50 percent," in *Proc. SPIE*, 2016, pp. 974304-1–974304-8. [Online]. Available: http://proceedings.spiedigitallibrary.org/proceeding.aspx?doi=10.1117/1 2.2218486

[25] D. Masson, F. Proulx, and S. Fafard, "Pushing the limits of concentrated photovoltaic solar cell tunnel junctions in novel high-efficiency GaAs phototransducers based on a vertical epitaxial heterostructure architecture," *Progress Photovolt.: Res. Appl.*, vol. 23, no. 12, pp. 1687–1696, 2015. [Online]. Available: http://doi.wiley.com/10.1002/pip.2709

[26] A. W. Walker *et al.*, "Impact of photon recycling and luminescence coupling on III-V photovoltaic devices," in *Proc. SPIE*, 2015, vol. 9358, pp. 11–13.

[27] J. F. Geisz, M. A. Steiner, I. García, R. M. France, D. J. Friedman, and S. R. Kurtz, "Implications of redesigned, high-radiative-efficiency GaInP junctions on III-V multijunction concentrator solar cells," *IEEE J. Photovolt.*, vol. 5, no. 1, pp. 418–424, Jan. 2015.

[28] M. A. Steiner, J. F. Geisz, I. García, D. J. Friedman, A. Duda, and S. R. Kurtz, "Optical enhancement of the open-circuit voltage in high quality GaAs solar cells," *J. Appl. Physics*, vol. 113, no. 12, 2013, Art. no. 123109. [Online]. Available: http://link.aip.org/link/JAPIAU/v113/i12/p123109/s1&Agg=doi

[29] M. Wilkins *et al.*, "Performance impact of luminescent coupling on monolithic 12-junction phototransducers for 12 V photonic power systems," in *Proc. SPIE*, Mar. 2016, vol. 9743, pp. 97430W-1–97430W-6. [Online]. Available: http://proceedings.spiedigitallibrary.org/proceeding.aspx?doi=10.1117/1 2.2213727

[30] M. M. Wilkins, C. E. Valdivia, A. M. Gabr, D. P. Masson, S. Fafard, and K. Hinzer, "Luminescent coupling in planar opto-electronic devices," *J. Appl. Physics*, vol. 118, no. 14, 2015, Art. no. 143102. [Online]. Available: http://scitation.aip.org/content/aip/journal/jap/118/14/10.1063/1.4932660
[31] F. Proulx *et al.*, "Measurement of strong photon recycling in ultra-thin GaAs n/p junctions monolithically integrated in high-photovoltage vertical epitaxial heterostructure architectures with conversion efficiencies exceeding 60%," *Physica Status Solidi–Rapid Res. Lett.*, vol. 6, pp. 1–4, 2016. [Online]. Available: http://doi.wiley.com/10.1002/pssr.201600385
[32] M. M. Wilkins and K. Hinzer, "Multi-junction Solar Cells," in *Handbook of Optoelectronic Device Simulation*, J. Piprek, Ed. New York, NY, USA: Taylor & Francis, 2017, ch. 40.
[33] S. L. Chuang, *Physics of Photonic Devices*, 2nd ed. Hoboken, NJ, USA: Wiley, 2009.
[34] R. R. King *et al.*, "Band gap-voltage offset and energy production in next-generation multijunction solar cells," *Progress Photovolt.: Res. Appl.*, vol. 19, pp. 797–812, 2011.
[35] C. Nayar, S. Islam, H. Dehbonei, K. Tan, and H. Sharma, "Power Electronics for Renewable Energy Sources," in *Power Electronics Handbook*, 3rd ed. Amsterdam, The Netherlands: Elsevier, 2007, ch. 28, pp. 673–716. [Online]. Available: http://dx.doi.org/http://linkinghub.elsevier.com/retrieve/pii/B9780120884797500456
[36] J. F. Geisz *et al.*, "Generalized optoelectronic model of series-connected multijunction solar cells," *IEEE J. Photovolt.*, vol. 5, no. 6, pp. 1827–1839, Nov. 2015.
[37] P. Crump *et al.*, "85% power conversion efficiency 975-nm broad area diode lasers at - 50C, 76 % at 10C," in *Proc. Conf. Lasers Electro-Optics Quantum Electron. Laser Sci. Conf.*, 2006, vol. 1, Art. no. JWB24.
[38] C. A. Hurni *et al.*, "Bulk GaN flip-chip violet light-emitting diodes with optimized efficiency for high-power operation," *Appl. Physics Lett.*, vol. 106, no. 3, 2015, Art. no. 031101. [Online]. Available: http://dx.doi.org/10.1063/1.4905873
[39] J. Nelson, *Physics of Solar Cells*. London, U.K.: Imperial College Press, 2003.
[40] G. L. Araújo and A. Martí, "Absolute limiting efficiencies for photovoltaic energy conversion," *Solar Energy Mater. Solar Cells*, vol. 33, no. 2, pp. 213–240, 1994.
[41] M. A. Green, "Limiting photovoltaic monochromatic light conversion efficiency," *Progress Photovolt.: Res. Appl.*, vol. 9, no. 4, pp. 257–261, 2001.
[42] B. Paquette *et al.*, "Optimization of p-doping in AlGaAs grown by CBE using TMA for AlGaAs/GaAs tunnel junctions," *J. Crystal Growth*, vol. 374, pp. 1–4, Jul. 2013. [Online]. Available: http://linkinghub.elsevier.com/retrieve/pii/S0022024813002340
[43] H. Moench *et al.*, "High-power VCSEL systems and applications," in *Proc. SPIE*, 2015, vol. 9348, pp. 93480W-1–93480W-10.
[44] J. Neely *et al.*, "Scaling power electronic converter SWaP based on WBG and UWBG device characteristics," in *Proc. Appl. Power Electron. Conf.*, San Antonio, TX, USA, 2016, pp. 1–25.
[45] Coherent Inc., "PulseLife CW horizontal array," Santa Clara, CA, USA, p. 2, 2009. [Online]. Available: http://dilas.com/assets/media/products/PulseLife-CW-Horizontal-Array-Da ta-Sheet.pdf
[46] J. Rabkowski, D. Peftitsis, and H.-P. Nee, "Silicon carbide power transistors: A new era in power electronics is initiated," *IEEE Ind. Electron. Mag.*, vol. 6, no. 2, pp. 17–26, Jun. 2012.
[47] J. Biela, M. Schweizer, S. Waffler, and J. W. Kolar, "SiC versus Si - Evaluation of potentials for performance improvement of inverter and DC-DC converter systems by SiC power semiconductors," *IEEE Trans. Ind. Electron.*, vol. 58, no. 7, pp. 2872–2882, Jul. 2011.
[48] H.-P. Nee, J. W. Kolar, P. Friedrichs, and J. Rabkowski, "Editorial: Special issue on wide bandgap power devices and their applications, 2014," *IEEE Trans. Power Electron.*, vol. 29, no. 5, pp. 2153–2154, May 2014.
[49] J. Rabkowski, "Power converters with silicon carbide devices," in *Proc. 14th Biennial Baltic Electron. Conf.*, Tallinn, Estonia, 2014, pp. 7–16.
[50] A. Anthon, Z. Zhang, and M. A. E. Andersen, "Comparison of a state of the art Si IGBT and next generation fast switching devices in a 4 kW boost converter," in *Proc. IEEE Energy Convers. Congr. Expo.*, Sep. 2015, pp. 3003–3011. [Online]. Available: http://ieeexplore.ieee.org/document/7310080/
[51] H. Li and M. N. Stig, "Challenges in switching SiC MOSFET without ringing," in *Proc. PCIM Eur. Conf. Proc.*, Nuremberg, Germany, 2014, pp. 989–994.
[52] Z. Zhang, B. Guo, F. F. Wang, E. A. Jones, L. M. Tolbert, and B. J. Blalock, "Methodology for wide band-gap device dynamic characterization," *IEEE Trans. Power Electron.*, vol. 32, no. 12, pp. 9307–9318, 2017.
[53] C. DiMarino, Z. Chen, M. Danilovic, D. Boroyevich, R. Burgos, and P. Mattavelli, "High-temperature characterization and comparison of 1.2 kV SiC power MOSFETs," in *Proc. IEEE Energy Convers. Congr. Expo.*, 2013, pp. 3235–3242.
[54] M. Ishigaki, S. Fafard, D. P. Masson, M. M. Wilkins, C. E. Valdivia, and K. Hinzer, "A new optically-isolated power converter for 12 V gate drive power supplies applied to high voltage and high speed switching devices," in *Proc. IEEE Appl. Power Electron. Conf. Expo.*, 2017, pp. 2312–2316. [Online]. Available: http://ieeexplore.ieee.org/document/7931022/
[55] A. Reinders, P. Verlinden, W. van Sark, and A. Freundlich, *Photovoltaic Solar Energy: From Fundamentals to Applications*. New York, NY, USA: Wiley, 2017.

Matthew M. Wilkins received the B.Sc. degree in engineering physics from Queen's University, Kingston, ON, Canada, in 2001. He received the M.Sc. degree in systems science in 2013, and the Ph.D. degree in electrical engineering in 2017, both from the University of Ottawa, Ottawa, ON, Canada.

For eight years, he was an Engineer with two small engineering companies related to the field of renewable energy technology, Flywheel Energy Systems Inc. and Magenn Power Inc. Since 2017, he has been a Postdoctoral Fellow with the University of Ottawa. His research focuses on intermediate-band materials for infrared photodetectors, as well as the development of photovoltaic power converters including advanced materials (dilute nitrides) and device simulations incorporating luminescent coupling phenomena.

Masanori Ishigaki received the B.S. degree in electrical engineering from Tokyo Metropolitan University, Tokyo, Japan, in 2005 and the M.S. degree in electrical and electronic engineering from Tokyo Institute of Technology, Tokyo, Japan, in 2007.

Since 2007, he has been with Toyota Central R&D Labs, Inc., Nagakute, Japan. His research interests include electrical systems for vehicle electronics and power converter circuits.

Dr. Ishigaki was a recipient of the IPEC 2010 Second Prize Paper Award, and the APEC 2012 and 2017 Outstanding Presentation Awards.

Philippe-Olivier Provost's photograph and biography not available at the time of publication.

Denis Masson was born in Rimouski, Canada. He received the Physics and the M.Sc. degrees from the University of Ottawa, Ottawa, ON, Canada, and the Ecole Polytechnique de Montreal, Montreal, QC, Canada. He received the Ph.D. degree in applied and engineering physics from Cornell University, Ithaca, NY, USA, in 1991.

He is specialized in the design and fabrication of optically active III-V compound semiconductor devices and has worked for Nortel and ST Micro-Electronics as well as startup companies such as MetroPhotonics, Cyrium Technologies, ArtIC Photonics, and Azastra Opto, where he was the co-founder. He currently works for Broadcom Ltd., Vancouver, BC, Canada.

Simon Fafard received the Ph.D. degree in physics from the University of Ottawa, Ottawa, ON, Canada, in 1992.

He was an NSERC Postdoctoral Fellow with the Center for Quantized Electronic Structures, University of California, Santa Barbara (UCSB). He is currently a Hardware specialist with Broadcom Semiconductor ULC, Vancouver, BC, Canada. Broadcom is a large public corporation that recently acquired Azastra, where Simon was a Co-founder and President. Azastra, an innovative III-V semiconductor corporation, commercialized laser power converter products based on the patented vertical epitaxial heterostructure architecture (VEHSA design) technology. He has been focused on the design, epitaxy, and characterization of optoelectronic devices at Université de Sherbrooke and at Azastra. As an entrepreneur, he cumulates more than 25 years of experience in optoelectronics and photonics while developing and commercializing numerous devices and products in the industry with Azastra, Aton, Cyrium, Alcatel Optronics, Kymata, and also in research labs as a Professor with Université de Sherbrooke, as a Senior Research Officer with National Research Council, as an Adjunct Professor in physics with the University of Ottawa, and with UCSB.

Dr. Fafard received the 2017 CAP Medal for Outstanding Achievement in Industrial and Applied Physics. He has an h-index of 46, with about 250 publications, with over 10 000 citations, and he is the inventor of more than 30 patents. He raised over $20M of private and venture capital funding and also obtained numerous research grants. He led Cyrium to become a manufacturer of one of the highest performance multijunction III-V solar cells and led Azastra to manufacture the highest performance phototransducer products.

Christopher Valdivia received the B.Sc. degree in computer engineering from the University of Manitoba, Winnipeg, MB, Canada, in 2001, the M.Sc. degree in electrical engineering from the University of Toronto, Toronto, ON, Canada, in 2003, and the Ph.D. degree from the Optoelectronics Research Centre, the University of Southampton, Southampton, U.K., in 2007.

Since 2007, his focus has been toward advancing high-efficiency photovoltaic devices and systems, starting with a Postdoctoral fellowship with the University of Ottawa's SUNLAB, followed by several years at multijunction solar cell startup Cyrium Technologies. He is currently a Senior Research Scientist with the University of Ottawa, Ottawa, ON, Canada. His research interests include photonic power converters, multijunction solar cells, energy yield modeling, and renewable energy generation.

Ercan M. Dede received the B.S. and the M.S. degrees in mechanical engineering from the University of Michigan, Ann Arbor, MI, USA and Stanford University, in 1998 and 2002, respectively. He received the Ph.D. degree in mechanical engineering from the University of Michigan, in 2007.

He is currently a Senior Research Manager with the Electronics Research Department, Toyota Research Institute of North America, Ann Arbor, MI, USA. His group focuses on advanced vehicle electronics involving next generation power semiconductors, advanced packaging, and thermal management technology. He holds more than 45 issued patents and has published more than 50 articles in archival journals and conference proceedings on topics related to the design and structural optimization of thermal-fluid, mechanical, and electromagnetic systems. He is an author of a book entitled *Multiphysics Simulation: Electromechanical System Applications and Optimization* (Springer, 2014).

Karin Hinzer (SM'15) received the B.Sc., M.Sc., and Ph.D. degrees in physics from the University of Ottawa, Ottawa, ON, Canada, in 1996, 1998, and 2002, respectively.

She is an Associate Professor with the School of Electrical Engineering and Computer Science with a cross-appointment with the Department of Physics, University of Ottawa. She has made pioneering contributions to the experimental physics of quantum dots marked by two landmark papers in science. She gained extensive experience in the design and fabrication of group III-V semiconductor devices while at the National Research Council Canada, Nortel Networks, and then Bookham (now Oclaro). Cost reduction strategies and liaison with remote fabrication facilities strongly feature in her industry experience. She joined the University of Ottawa in 2007 where she founded the SUNLAB, the premier Canadian modeling and characterization laboratory for next generation multijunction solar devices and concentrator systems. With its designation as a University of Ottawa Core Facility and its close integration with the Centre for Research in Photonics, the SUNLAB leverages its resources for collaborations with other research groups from within the university and the rest of the world, as well as with industrial partners. Her research involves developing new ways to harness the suns energy. She is the Principal Investigator of the new NSERC CREATE Training in Optoelectronics for Power: From Science and Engineering to Technology program, a multidisciplinary training program involving three universities and aiming to train over 100 students in six years. She has published more than 150 refereed papers, trained more than 110 highly qualified personnel and her laboratory has spun-off three Canadian companies in the energy sector. Her research interests include new materials, high efficiency light sources and light detectors, solar cells, solar modules, new electrical grid architectures, and voltage converters.

Prof. Hinzer was the Tier II Canada Research Chair in Photonic Nanostructures and Integrated Devices from 2007 to 2017. In 2010, she was the recipient of the Inaugural Canadian Energy Award with industry partner Morgan Solar for the development of more efficient solar panels. In 2015, she received the Ontario Ministry of Research and Innovation Early Researcher Award for her contributions to the fields of photonic devices and photovoltaic systems and in 2016, she was the recipient of the University of Ottawa Young Researcher Award. She is a member of the College of New Scholars, Artists and Scientists of the Royal Society of Canada.